Evaluation of the physical mechanisms of adhesively bonded metal-based hybrid material systems under tensile loading

D. Hummelberger, L. Kärger, Kay A. Weidenmann, J. Staeves, F. Henning

Angaben zur Veröffentlichung / Publication details:

Hummelberger, D., L. Kärger, Kay A. Weidenmann, J. Staeves, and F. Henning. 2017. "Evaluation of the physical mechanisms of adhesively bonded metal-based hybrid material systems under tensile loading." *Materials and Design* 132: 215–24. https://doi.org/10.1016/j.matdes.2017.07.001.

Evaluation of the physical mechanisms of adhesively bonded metal-based hybrid material systems under tensile loading

D. Hummelberger[a, c, *], L. Kärger[a], K.A. Weidenmann[b], J. Staeves[c], F. Henning[a]

[a] *Karlsruhe Institute of Technology (KIT), Institute of Vehicle System Technology (FAST), Lightweight Technology (LBT), Karlsruhe, Germany*
[b] *Karlsruhe Institute of Technology (KIT), Institute of Applied Materials (IAM), Karlsruhe, Germany*
[c] *BMW Group, Research and Innovation Centre (FIZ), Munich, Germany*

[*] Corresponding author.
E-mail address: david.hummelberger@kit.edu (D. Hummelberger).

1. Introduction

Hybrid material systems are created by the specific combination of materials from different classes, levels and/or sub-levels [1,2]. As a result, complex property profiles can be achieved which cannot be attained by monolithic material solutions. Despite the fact that hybrid materials are already partly in series in different industries, a comprehensive understanding for the specific selection and combination of materials of the composite is still lacking in many areas. As a consequence, the potential of hybrid composite materials cannot be fully utilized. For a more efficient design of future lightweight structures, a profound knowledge of the interaction of the individual components of the hybrid material system is essential.

One of the first studies on the quasi-static tensile behavior of laminated metal composites (LMCs) combining ultrahigh carbon steel (UHCS) with 304 stainless steel, Hadfield manganese steel or Fe-3%Si alloy is presented by Lee et al. [3]. They performed tensile tests on roll bonded laminates after different conditions of selective heat treatment. The combination of UHCS and 304 stainless steel results in about doubled elongation at break in comparison to the single UHCS. However, the ductility of monolithic 304 stainless steel is far from being achieved [3].

In addition, the improvement of ductility of roll bonded laminates containing steel sheets is presented inter alia by Bouaziz et al. [4], Syn et al. [5], Koseki et al. [6], Inoue et al. [7] and Lesuer et al. [8]. Two-layered LMCs containing martensitic steel and high manganese twinning-induced plasticity (TWIP) steel result in high yield strength and especially high uniform elongation [4]. An improvement of tensile ductility and strength can also be attained by composites constructed of UHCS and brass [5], of high strength (martensitic) steel and high ductility (austenitic or low carbon) steel [6,7] as well as magnesium alloy and austenitic steel [6]. An enhancement of elongation at break with decreased layer thickness is presented by Syn et al. [5] and Inoue et al. [7]. According to Ref. [5], this effect of the layer thickness is attributed to residual stress whose influence on delamination is reduced with decreasing layer thickness.

The tensile behavior of laminates based on steel and aluminum sheets is examined by Semiatin et al. [9]. The stable and unstable plastic flow of three-layered stainless steel-clad aluminum and aluminum-clad stainless steel sandwich sheet materials is evaluated with uniaxial tensile tests. The tensile ductility is between the characteristic values of the two monolithic materials of the hybrid solution. In addition, unstable deformation occurs due to the necking of the layers and delamination arises through the plasticity-induced thinning of the individual layers [9].

First investigations on strain fields as well as the stress partitioning of roll bonded laminates containing steel sheets are presented inter alia by Lhuissier et al. [10], Nambu et al. [11] and Ojima et al. [12]. In Ref. [10], the strain fields are investigated for laminates constructed of 13 alternating layers of high-carbon steel (SUS420) and ductile steel (SUS301). The significantly improved tensile ductilities are attributed to the macroscopically homogenous strain field across the specimens. Thus, in the martensitic steel the onset of failure is delayed [10,11]. Stress partitioning in LMCs containing martensitic and austenitic layers was investigated during uniaxial tensile tests with in situ neutron diffraction measurements by Ojima et al. [12]. According to Ref. [12], the deformation mode is divided into three stages, a fully elastic, a partially plastic as well as a fully plastic stage. However, no detailed optical strain and thermography measurements as well as comprehensive numerical studies for the evaluation of the interaction between the constituents and the related mechanisms are performed.

Most of the mentioned investigations are performed on laminates processed by roll bonding or deposition. A study on the influence of bonding strength of the laminate interface on tensile ductilities of LMCs containing martensitic steel and austenitic steel is presented by Nambu et al. [13]. Comparative measurements of roll bonded and adhesively bonded sheet metal laminates are presented [13]. For this specific laminate, they found out, that with increasing bonding strength, improved increased tensile ductility can be achieved [13]. Nevertheless, the influence of the stiffness or the elongation at break of the intermediate adhesive layer on the interaction between the individual components of the laminate is not examined by Nambu et al. [13].

The present paper systematically analyzes and assesses selected hybrid material systems consisting of adhesively bonded sheet metals as well as their underlying physical mechanisms at uniaxial tensile loading. For the purposeful assessment of different underlying mechanisms, hybrid materials constructed of Interstitial-Free (IF) steel and twinning-induced plasticity (TWIP) steel as well as solutions consisting of IF steel with the aluminum alloy EN-AW 5182-O are selected. To investigate the interaction between their constituents systematically, structural adhesives with different stiffness and elongation at break levels are used for the adhesive bonding. In addition, hybridization-induced mechanisms for the targeted stabilization of plastic instabilities are evaluated in detail with complementary optical strain measurements, thermography and numerical simulation. By consistent implementation of a design strategy based on these underlying mechanisms, the ductility and also the tensile strength of such material combinations can be adjusted. Hence, locally tailored properties according to the local requirements can be obtained by hybridization of a cost-effective base structure with reinforcing patches.

2. Materials

2.1. Metals

In the course of this work, three different sheet metals are used to investigate the underlying physical mechanisms of different hybrid material systems systematically. An Interstitial-Free (IF) steel HC220Y, which is widely applied in the automotive industry, is used. The HC220Y has been produced by ThyssenKrupp Steel and is abbreviated as “HC” in the following. Furthermore, EN AW 5182-O (abbreviated as “AL”), a standard aluminum-magnesium alloy for body parts, is applied. This aluminum alloy has been provided by Constellium. In addition, an optimized twinning-induced plasticity (TWIP) steel (HSD®-steel X70MnAlSi15_2.5_2.5) from Salzgitter Mannesmann Forschung GmbH is used and is abbreviated as “HSD” (High Strength and Ductility) in the following. The investigated metals have a layer thickness of about 1.0 mm. The measured mechanical characteristics of the individual materials under quasi-static loading conditions are shown in Table 1.

2.2. Adhesives

Epoxy resin based cold-curing structural adhesives from Dow Automotive with a thickness of 0.15 mm are used for the adhesive bonding between the individual materials. The influence of adhesive stiffness and elongation at break on the interaction of the components of the hybrid material system is evaluated by using the structural adhesives which are listed in Table 2. The Betamate 2090 2:1 [14], which is abbreviated as “BM21” in the following, possesses high Young’s modulus compared to Betamate 2090 1:1 (abbreviated “BM11”) [15]. A complete parameter set, which is essential for numerical simulation, was not available for the experimentally tested BM11 and BM21. Therefore, BETAMATE 2098 (abbreviated as “BM98”) [16] is applied for the numerical simulations.

Table 1
Measured quasi-static properties of the applied materials.

Name	Ultimate tensile strength	0.2% proof stress	Uniform elongation	Elongation at break	Young's modulus
	σ/MPa	$R_{p0,2}$/MPa	ε_p/%	ε_f/%	E/GPa
HC220Y	375 ± 2	230 ± 1	23.01 ± 0.33	36.4 ± 0.9	202 ± 7
EN AW 5182-O	289 ± 1	137 ± 1	24.15 ± 0.77	26.0 ± 0.4	70 ± 1
X70MnAlSi15_2.5_2.5	1027 ± 4	546 ± 1	49.46 ± 0.34	53.4 ± 0.4	182 ± 3

Table 2
Properties of the applied adhesives [14–16] .

	DIN EN 1465	DIN EN ISO 527-1		
Name	Lap shear strength/MPa	Ultimate tensile strength/MPa	Elongation at break/%	Young's modulus/MPa
BM 2090 1:1 [20] (BM11)	18	16	$\geq$ 84	150
BM 2098 [21] (BM98)	23	22	$\geq$ 20	1100
BM 2090 2:1 [19] (BM21)	25	30	$\geq$ 5	2000

2.3. Evaluated monolithic materials and hybrid material systems

In the course of this work, the type of metal as well as the adhesive layer serve as variation parameters. These parameters are summarized in Table 3 in terms of the investigated configurations of the experimental and the basic numerical program. The hybrid specimens are three-layered metal laminates joined with the specified structural adhesives.

In order to realize an excellent adhesive bond, the surface of the sheet metals are ground and also cleaned with isopropyl alcohol. The application of the adhesive to the sheet metals is performed with a 2 K cartridge pistol for 2 K structural adhesives. The individual layers are pressed with a Collin laboratory platen press under constant conditions. After pressing, the hybrid material systems were put into a separate pressing tool to ensure that the adhesive layer is cured at room temperature under constant pressure. After seven days curing at room temperature, the test specimens were extracted by high precision waterjet-cutting according to DIN 50125 type H [17] with a gauge length of 80 mm from the plate. Furthermore, the specimens are finished by milling to ensure the required surface quality in thickness direction.

3. Methods

3.1. Experimental setups and test procedures

A Zwick universal testing machine with a 200 kN load cell at the Institute of Applied Materials (IAM) at the Karlsruhe Institute of Technology, is used for all material characterization experiments which are described in the following. To measure the strains, a multiXtens as well as an optical strain measurement system, consisting of Canon EOS 70D and MATLAB-based digital image correlation (DIC) software, are installed. The deformation as well as onset and progress of the localization of strain can be visualized on the basis of strain distribution contours. Furthermore, these deformation processes cause a temperature change [18]. Therefore, a FLIR Systems GmbH thermal imaging camera, referred to as T420, is used. By complementary optical strain measurements and thermography, the different strengthening and local failure mechanisms and especially the hybridization-induced changes of these mechanisms in comparison to the constituents are examined in detail.

All tensile tests on the sheet metals as well as on the hybrid material systems consisting of sheet metals are performed according to DIN EN ISO 6892-1 [19]. In accordance with these standards, different crosshead velocities for the different test phases are used. For the determination of Young's modulus by regression according to DIN EN ISO 6892-1 [19], a nominal strain rate of 7×10^{-5} 1/s and different evolution ranges for the different materials in accordance with the standards are selected. A nominal strain rate of 25×10^{-5} 1/s is used for the test phase until yield strength. In the field of higher strains, the strain rate is increased to 2×10^{-3} 1/s.

3.2. Numerical modeling

The numerical investigations are performed by using the commercial ABAQUS/Explicit finite element code. For modeling, the uniaxial tensile behavior of the monolithic metal specimens and the hybrid specimens, 3D models (specimen type H according to DIN 50125 [17]) are developed. The sheet metals are discretized by solid elements (C3D8 elements). The adhesive joints of the hybrid

Table 3
Composition of the investigated monolithic materials and hybrid configurations.

Classification	Configuration	Component 1	Component 2	Adhesive
		(1.0 mm)	(1.0 mm)	(0.15 mm)
References	HC220Y (HC)	HC	–	–
	EN AW 5182-O (AL)	AL	–	–
	X70MnAlSi15_2.5_2.5 (HSD)	HSD	–	–
Hybrids	AL-BM11-HC-BM11-AL	HC	AL	BM11
	AL-BM98-HC-BM98-AL	HC	AL	BM98
	AL-BM21-HC-BM21-AL	HC	AL	BM21
	HSD-BM11-HC-BM11-HSD	HC	HSD	BM11
	HSD-BM98-HC-BM98-HSD	HC	HSD	BM98
	HSD-BM21-HC-BM21-HSD	HC	HSD	BM21

material systems are modeled by using cohesive elements (COH3D8 elements) [20].

The material model for the metals is a linear elastic model expanded by a plasticity model with isotropic von Mises yield function. To describe the failure behavior, a IDS failure criteria presented by Hooputra et al. [21] is applied. This is a phenomenological model for ductile and shear fracture and is already implemented in ABAQUS/Explicit [20]. For the plasticity model of the three metal sheets, the hardening curve during plastic deformation up to uniform elongation is described directly by the stress vs. strain curves of the experimental uniaxial tensile tests. The extrapolation of the hardening curve beyond uniform elongation is described by Swift-Voce law [22,23]. The material constants describing these two laws are identified by parameter optimization procedure based on the least squares method and using the hardening curves generated from experiments. To model the diffuse and localized necking behavior of the HC layer exactly, the plasticity model has to be extended by strain rate dependent material data [24–27]. The strain rate dependent hardening curves of the HC are determined by scaling the original curve with the strain rate sensitivity m according to Hart et al. [24]. This parameter m of the HC as well as the parameters for ductile and shear fracture of the different metals are identified based on former experimental data of the BMW Group. In the final report of FOSTA P 957 [28], the required parameter for the cohesive zone model are determined for the structural adhesive BM98.

4. Results

4.1. Experimental and numerical results of AL-HC-AL-hybrids

Fig. 1a depicts the experimental engineering stress vs. engineering strain curves of two AL-HC-AL-hybrid specimens with different adhesives (solid blue and solid green) in comparison to curves of the two monolithic materials, AL (black) and HC (grey). In general, the curve progression of the two hybrid material systems can be divided into four regions following the phenomenological description according to Kelly [29]. A linear elastic behavior is followed by a region in which one material shows linear elastic behavior, whereas in the second material plastification occurs. Subsequently, the following region is determined by plastification of both materials. After the failure of the first material, plastic behavior of the remaining material can be observed. Comparing the curves of the hybrids containing the two different structural adhesives, a difference in uniform elongation can be recognized, whereas a good agreement for elongation at break can be seen. The stepped failure behavior is more pronounced at the hybrid containing the adhesive BM21 which offers a higher stiffness and smaller elongation at break of the adhesive. Compared to monolithic AL, both hybrids exhibit about 5% higher elongation at break.

Yield strength, hardening behavior, ultimate tensile strength and uniform elongation observed in experiments show a good correlation with simulation results for the monolithic materials HC (dashed grey) and AL (dashed black) as well as the AL-HC-AL-Hybrid (dashed light green).

Looking in detail at the experimentally and numerically observed curve progression of AL and also of the two AL-HC-AL-Hybrids, a serrated stress vs. strain behavior can be detected (detail in Fig. 1a). The serrated curve progression can be attributed to the Portevin-Le Chatelier (PLC) effect. This effect is ascribed to dynamic strain aging, which refers to dynamic interactions between dislocations and mobile solute atoms [30,31]. Further, it can be observed that AL shows a more pronounced sawtooth-shaped behavior compared to hybrid material systems. The strain paths of the critical (highest strain) elements of the monolithic materials HC (grey) and AL (black) as well as of the individual layers of the hybrid material solution (HC— blue, AL — green) are presented in Fig. 1b by equivalent plastic strain ε_{eq} vs. stress triaxiality η curves. The dimensionless parameter stress triaxiality η describes the stress state and is defined as the ratio of hydrostatic stress σ_h and equivalent von Mises stress σ_{eq} according to Hooputra et al. [21], Bao et al. [32,33] and Wierzbicki et al. [34]. Looking at the curves, differently pronounced shifts from the uniaxial strain path ($\eta = \sigma_h/\sigma_{eq} = 1/3$) can be detected for the different materials and the layers of the hybrid. Furthermore, serrated strain paths can be observed for aluminum as well as both constituents of the AL-HC-AL-hybrid, whereas monolithic HC shows a smooth curve progression.

Comparing the occurring mechanisms that are observed qualitatively by optical strain measurements, thermography and numerical simulation of the two monolithic materials HC and AL as well as the AL-HC-AL-hybrids (Fig. 2a–c), three different effects can be seen. On the one hand, HC shows the typical localized neck formation behavior at the center of the gauge area. On the other hand, localized deformation bands, referred to as PLC bands [30], become visible at AL. Looking at the progressing of these band-shaped deformations in experiment and simulation, it becomes evident, that they move

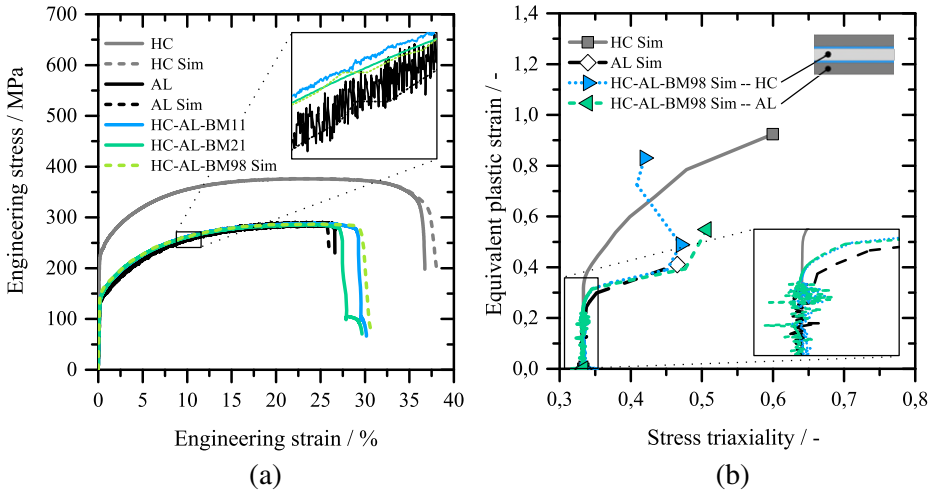

Fig. 1. a) Engineering stress vs. engineering strain curves for HC, AL and AL-HC-AL-hybrids and b) numerically predicted equivalent plastic strain paths of HC, AL and the individual layers of the AL-HC-AL-hybrid within the critical (highest strain) elements of the FE model.

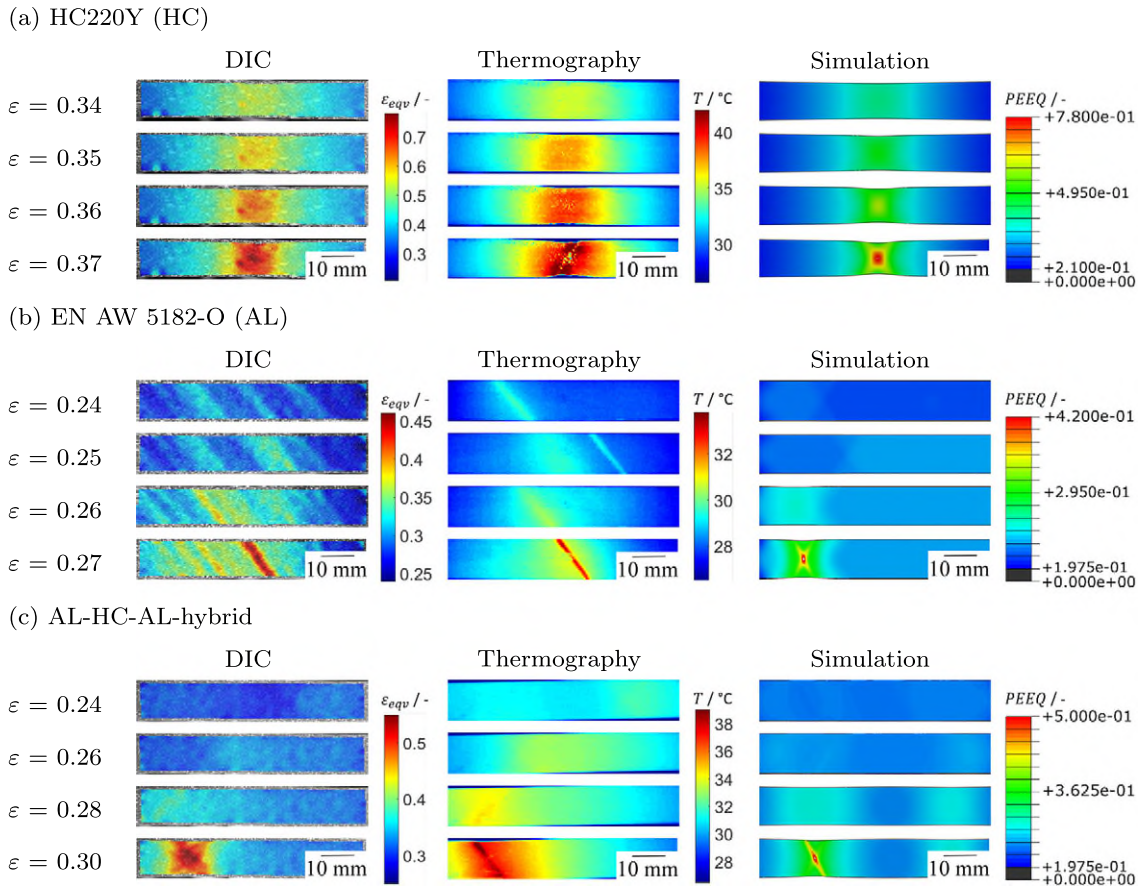

Fig. 2. Strain map from optical strain measurements (left); heat map from thermography (middle); distribution of equivalent plastic strain (PEEQ) in simulation (right) for a) HC, b) AL and c) AL-HC-AL-hybrids.

rapidly and discontinuously across the specimen. For hybrid solutions containing two layers AL and a single intermediate layer HC, slowly and continuously progressing wider bands become visible in contrast to the monolithic aluminum sheet metal.

4.2. Experimental and numerical results of HSD-HC-HSD-hybrids

The engineering stress vs. engineering strain curves of the monolithic HC (grey) and HSD (black) specimens as well as of the hybrid material systems, containing two outer HSD layers and an intermediate HC layer, are presented in Fig. 3a. Looking at the curves, it becomes evident, that the two hybrids with two different adhesives (solid blue and solid green) show nearly the same elongation at break (about 55%) as the monolithic HSD specimen. In comparison to AL-HC-AL-hybrids (Section 4.1), uniform plastic deformation until failure can be detected for the HSD-HC-HSD-hybrids, whereas the hybrids containing aluminum show the mentioned stepped failure behavior. This means that the intermediate HC layer, which usually shows about 35% elongation at break, is now forced to deform until about 55% due to the constraining effects of the adjacent outer HSD layers.

Looking at the numerical results of the hybrid material system containing BM98 (dashed light green) in Fig. 3a, it becomes evident that in comparison to the experimental results of the hybrid material systems containing BM11 (solid blue) and BM21 (solid green), a very good agreement can be achieved for yield strength, hardening behavior, ultimate tensile strength, uniform elongation as well as elongation at break.

The equivalent plastic strain ε_{eq} vs. stress triaxiality η curves of the constituent materials HC (grey) and HSD (black) as well as of the individual layers of the hybrid material solution (HC — blue, HSD — light green) are presented in Fig. 3b. Looking at the curves in detail, the monolithic HSD as well as the HSD layers of the HSD-HC-HSD-hybrid show a predominantly uniaxial strain path ($\eta = 1/3$), whereas for the monolithic HC an early drift and for the HC layer of the hybrid a significantly later drift to a multiaxial strain path can be detected.

By using optical strain measurements, thermography as well as numerical simulation, the strengthening mechanisms of HC, HSD and HSD-HC-HSD-Hybrids can be detected qualitatively in detail. Comparing the formation of localized necking of Fig. 4a–c, HC, HSD and laminates consisting of HSD and HC layers qualitatively show the same localized necking mechanisms. Looking in detail at the temporal progressions, the following behavior can be observed. HC shows less stable deformation (until about $\varepsilon = 0,23$), followed by slow localized neck formation, while HSD as well as the constructed hybrids exhibit a longer uniform elongation (until about $\varepsilon = 0,50$) followed by an abrupt localization of the strain.

5. Discussion

5.1. Tensile behavior of AL-HC-AL-hybrids

The more pronounced serrations in engineering stress vs. engineering strain curves of AL (Fig. 1a), which are mentioned in Section 4.1, are associated with random initiation and hopping propagation of localized deformation bands along the specimen length

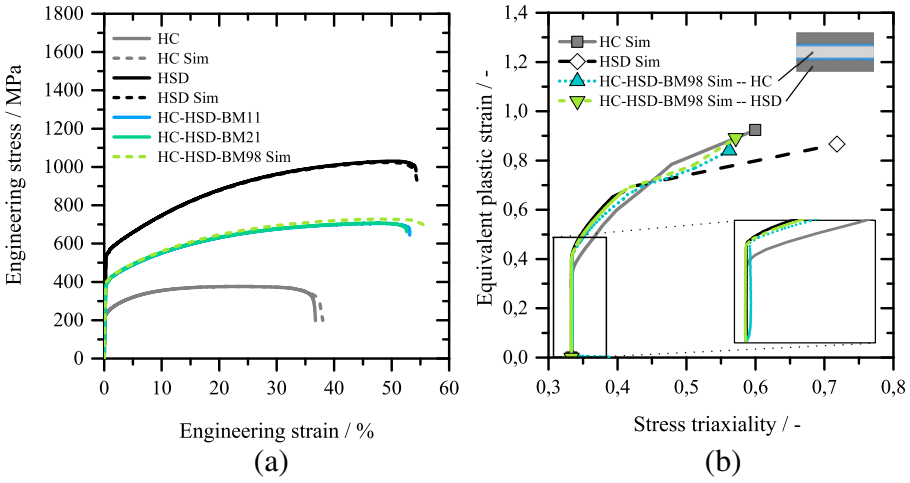

Fig. 3. a) Engineering stress vs. engineering strain curves for HC, HSD and HSD-HC-HSD-hybrids and b) numerically predicted equivalent plastic strain paths of HC, HSD and the individual layers of the HSD-HC-HSD-hybrid within the critical (highest strain) elements of the FE model.

(Fig. 2b, Fig. 5a). This type of PLC bands is referred to as type C according to Halim et al. [30].

In contrast, at hybrid material systems consisting of two aluminum layers with an intermediate steel layer, the wider localized deformation bands nucleate at one end of the gauge length of the specimen and propagate slowly, repetitively and continuously along the length of the specimen (Figs. 2c, 5 b). It seems that by hybridization a change of the type of PLC bands is caused in the AL layers. According to Halim et al. [30] this continuous propagation of the bands is referred to as type A. The resulting serrations are less pronounced (Fig. 1a) compared to those of the monolithic aluminum sample. The underlying physical mechanism of the hybrid material system which is responsible for the change of the type of PLC bands for the aluminum layer could be the so-called supporting or bridging effect [8,35]. This mechanism has

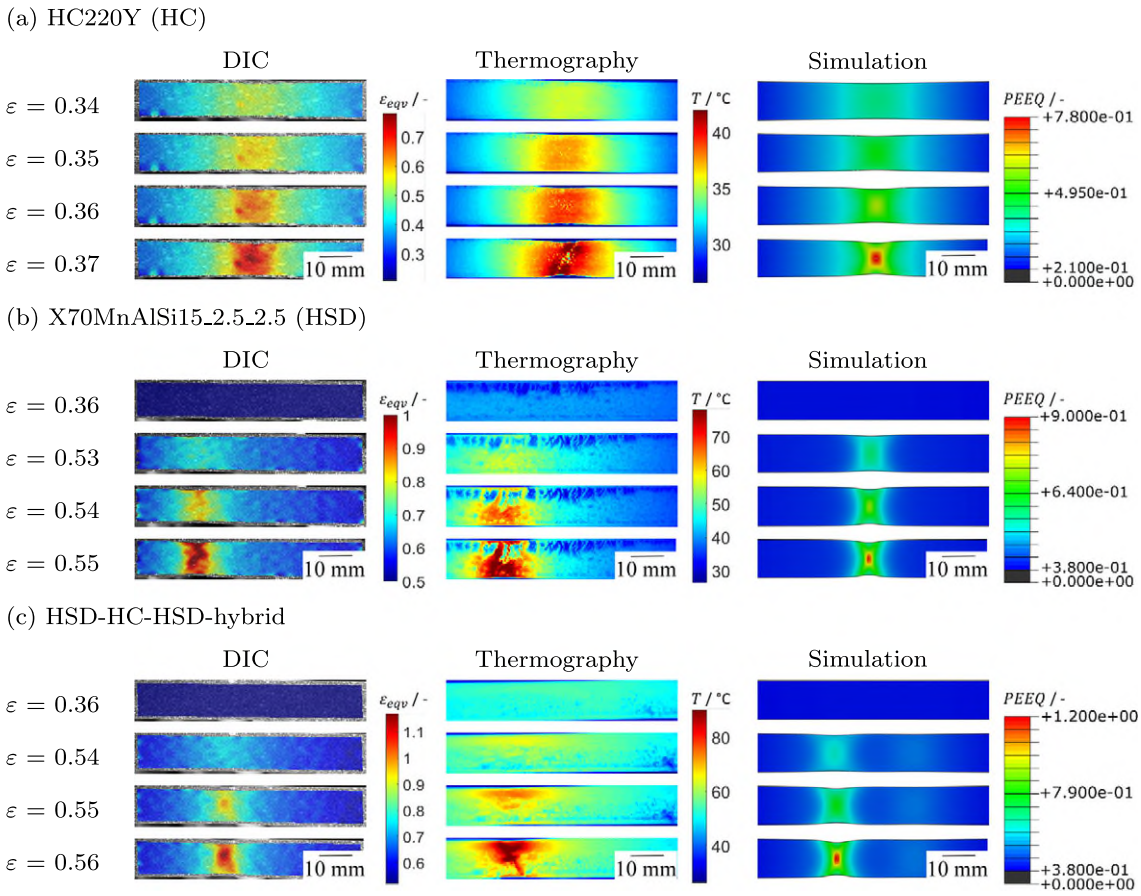

Fig. 4. Strain map from optical strain measurements (left); heat map from thermography (middle); distribution of equivalent plastic strain (PEEQ) in simulation (right) for a) HC, b) HSD and c) HSD-HC-HSD-hybrids.

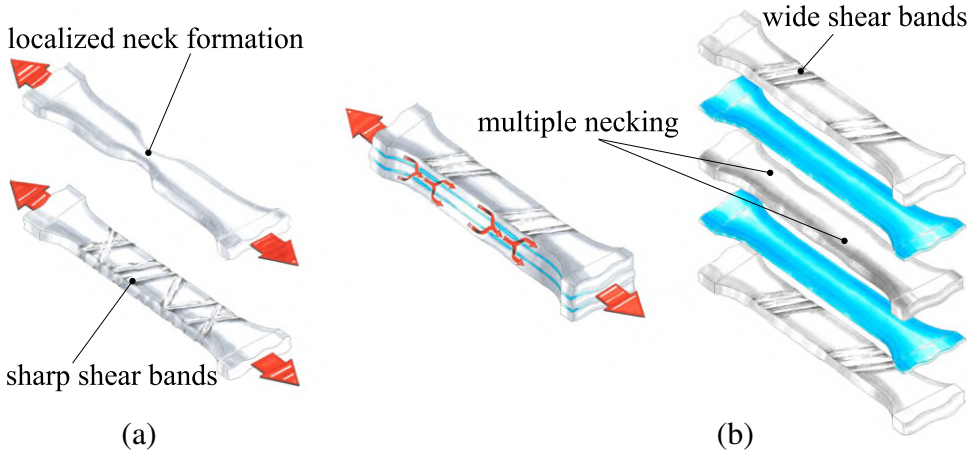

Fig. 5. Phenomenological description of the physical mechanisms of a) the monolithic materials (HC-at the top, AL-at the bottom) and b) the AL-HC-AL-hybrid (on the left) and the individual layers (on the right).

been observed in a 35-layer UHCS/brass laminated composite in terms crack growth resistance at bending load cases by Ohashi et al. [36] and in fiber metal laminates made of a low-ductility aluminum alloy and aramid fiber reinforced polypropylene at tensile load cases by Gonzalez-Canche et al. [37]. Fig. 5b depicts schematically, that in the area of softening at the individual serrations, the load can be transmitted to the adjacent steel layer. Hence, the drop in the curve is intercepted by hardening behavior of the supporting steel layer. At the areas of PLC bands within the AL layers, localized necking occurs in the intermediate HC layer. Thereby, the continuous propagation of the PLC bands leads to multiple necking within the steel layer (Fig. 5b). The effect of multiple necking is detected for spring steel wire reinforced aluminum profiles by Merzkirch et al. [38,39]. These mentioned effects can also be detected at the numerically calculated strain paths of the individual layers of the hybrid material system and the monolithic specimens (Fig. 1b). While in the single HC specimen a continuous uniaxial strain path ($\eta = 1/3$) until localized necking can be recognized, the intermediate HC layer of the AL-HC-AL-hybrid shows serrations in the strain path which correlate to those of the outer aluminum layers of the hybrid.

In addition, the neck formation of the outer aluminum layers, starting for monolithic aluminum at uniform elongation of about 24%, is hindered by the intermediate steel layer [10,11]. Due to the constraining effect caused by the intermediate HC layer, the strain path of the AL layers is changed by hybridization (Fig. 1b). Due to neck formation, the strain path drifts from uniaxial to multiaxial, in monolithic aluminum sheet. By reason of the mentioned localization hindrance, the aluminum layers of the hybrid are held slightly longer on the strain path of HC before they drift off.

The mentioned stepped failure behavior varies significantly comparing the curves of the hybrids containing the two different structural adhesives. At the hybrid containing the adhesive BM21 the metal layers separate at smaller strain and, based on that, the mechanism localization hindrance is ceased to be effective. Hence, localized necking is initiated for the aluminum layers, which results in an earlier stress drop. The HC-layer still carries the load and enables an elongation at break comparable to the hybrid with the adhesive BM11, however. At the hybrid joined with the BM11 the adhesive bonding remains longer, the aluminum layers are held on the strain path of HC nearly until total failure of the material composite.

In summary, the bridging effect, the multiple neck formation as well as the localization hindrance contribute to a change in the strain path of the individual layer and, consequently, to a 5% improvement of the elongation at break for these AL-HC-AL-hybrids in comparison to the monolithic aluminum. The manifestation of localization hindrance and thereby the stepped failure behavior can be influenced by the applied structural adhesive. For hybrids containing the adhesive with low stiffness, the adhesive bonding remains slightly longer and this results in higher uniform elongation of this hybrid, whereas the layers joined with the stiffer adhesive separate at smaller strains resulting in a more pronounced stepped failure behavior.

5.2. Tensile behavior of HSD-HC-HSD-hybrids

The uniform plastic deformation until failure of the HSD-HC-HSD-Hybrid at about 55% elongation is associated with the two distinctively different interacting physical mechanisms, localization hindrance and bridging effect, which result in the stabilization of plastic instabilities of the intermediate HC layer [10,11]. While the monolithic HC sheet metal is only deformed uniformly to an elongation of about 23%, the HSD shows a stable tensile deformation of up to 50% elongation (Figs. 3a, 6a). In the case of the HC, a small change in the cross-sectional area of the specimen occurs after the uniform deformation at one point along the length of the specimen, which results in a localization of the strain in this region. Hence, the strain is becoming more and more localized, a softening and, subsequently, the ultimate failure of the material occurs [24,25]. In the HSD-HC-HSD-hybrid, the larger stable tensile deformation of HSD is utilized. The outer HSD layers of the hybrid material attempt to suppress this localized neck formation in the HC layer and force the intermediate layer to deform still uniformly along the specimen length (Fig. 6b).

Lhuissier et al. [10], Semiatin et al. [9] and Ojima et al. [12] have assumed that such an effect is responsible for the improvement in elongation at break. This mechanism can also be described by comparing the numerically evaluated strain paths of the individual layers of the hybrid solution with those of the constituent materials. Fig. 3b shows that a uniaxial strain path ($\eta = 1/3$) is impressed to the intermediate layer of such a structure for a longer time. While the strain path of the individual HC layer drifts away from uniaxial to multiaxial above uniform elongation, the HC layer within the hybrid is kept on the uniaxial strain path until onset of plastic instability of the outer HSD layers. Consequently, no stepped failure behavior according to Kelly [29] can be detected, however, there is a behavior similar to that described by Ojima et al. [12].

The bridging effect as a second mechanism contributes to stabilize plastic instabilities [8,35]. In the area where the HC layer is reaching onset of necking, the surrounding HSD layers form a second load path and, subsequently, the load can be transmitted through

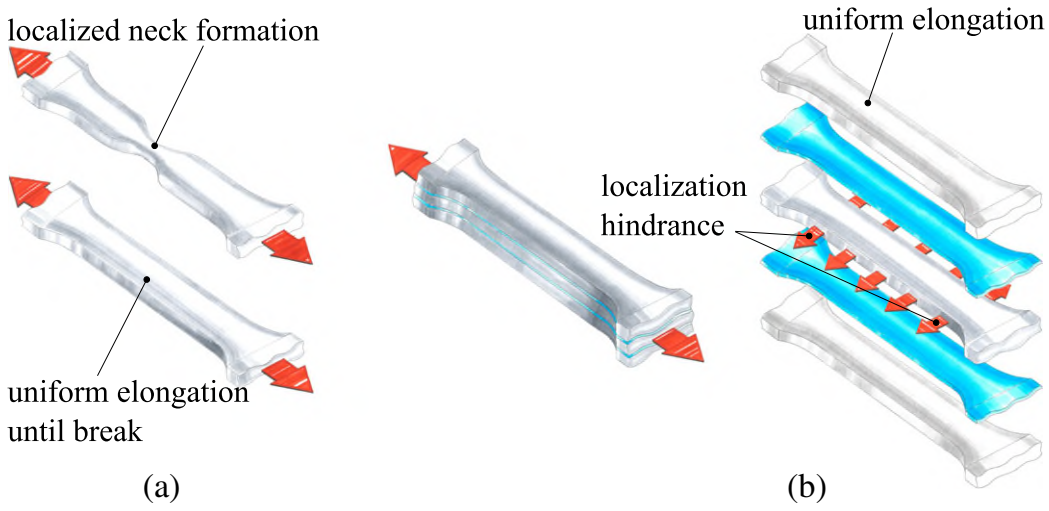

Fig. 6. Phenomenological description of the physical mechanisms of a) the monolithic materials (HC-at the top, HSD-at the bottom) and b) the HSD-HC-HSD-hybrid (on the left) and the individual layers (on the right).

this bridging load path [8,35,36]. By this redirection of the loads in the adjacent uniformly deforming layers, a discharge in the vicinity of the potential necking area occurs in the HC layer.

In comparison to the AL-HC-AL-hybrids, no significant influence of the adhesive properties on the deformation and failure behavior of the investigated material systems can be detected for the HSD-HC-HSD-hybrids.

In summary, the two physical mechanisms, localization hindrance and bridging effect, contribute to a change in the strain path of the intermediate HC layer, to stabilization of plastic instability in this layer and, based on that, to enlarged stable tensile deformation. As a result, a considerable improvement in the uniform elongation as well as in the elongation to break (up to 20% improvement) can be achieved by this type of hybridization.

5.3. Influencing factors on the mechanism localization hindrance

Due to the consistency of the experimental and numerical results regarding tensile strength, uniform elongation and elongation at break, the presented simulation methodology is used in the following to evaluate the influence of further variation parameters on the manifestation of the mechanism localization hindrance. In the course of this complementary numerical study on hybrids consisting of HC and HSD layers, the thickness of reinforcing HSD layer as well as the configuration of the hybrid material system serve as additional variation parameters.

The numerically predicted engineering stress vs. engineering strain curves of monolithic HC and HSD as well as of two- or three-layered hybrid material systems, consisting of an HC (1.0 mm) and HSD with varying thickness (1.0 mm, 0.6 mm, 0.2 mm), are presented in Fig. 7a and b. Looking at the curves of the hybrids in Fig. 7a, it becomes evident, that by hybridization of HC with HSD of the thickness 1.0 mm or 1.0 mm the elongation at break of the monolithic HSD (about 55%) can achieved. In comparison to these solutions, the hybrid containing an intermediate HC layer (1.0 mm) and two 0.2 mm thick HSD layers deform uniformly until about 50% elongation, however the ductility of monolithic HSD cannot be achieved. Comparing the two-layered hybrid material systems (Fig. 7b), the elongation at break of the monolithic HSD can only be attained with the 1.0 mm thick HSD layer. For the other two single-sided reinforced variants a reduction of ductility with decreasing thickness of the reinforcing HSD layer can be detected. The low stress values of the hybrid containing 0.2 mm thick

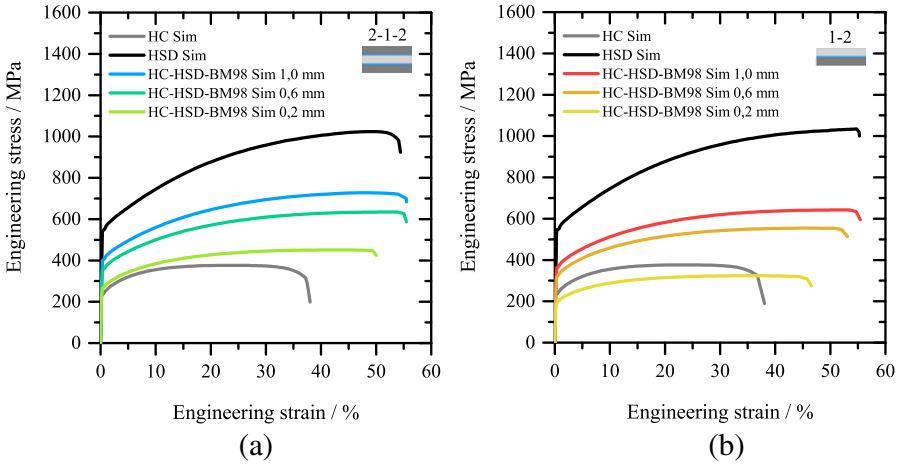

Fig. 7. a) Numerical engineering stress vs. engineering strain curves for HC, HSD and HSD-HC-HSD-hybrids (2-1-2-configuration) with different thickness of the HSD (1.0 mm, 0.6 mm, 0.2 mm) and b) numerical engineering stress vs. engineering strain curves for HC, HSD and HC-HSD-hybrids (1-2-configuration) with different thickness of the HSD (1.0 mm, 0.6 mm, 0.2 mm).

HSD compared to the monolithic HC are due to the fact that, for the calculation of the cross-sections, the thickness of the adhesive layer is taken into account.

Studies on both configurations show that especially the thickness of the reinforcing HSD layers is decisive for the onset of plastic instability in the HC layer and thereby for the achievable ductility of the hybrid. Below a certain thickness ratio, the reinforcing effect of the HSD layer is no longer sufficient to prevent the localized necking within the HC layer. Hence, plastic instability occurs within this layer and failure of the hybrid is initiated.

6. Conclusions

In this contribution, hybrid material systems consisting of different sheet metals are analyzed and assessed by uniaxial tensile tests. The occurring strengthening, localization and failure mechanisms and especially the hybridization-induced changes of the material-specific mechanisms are investigated by optical strain measurements, thermography and numerical simulation.

For hybrid material systems containing an intermediate layer of HC and two top layers of AL, the mechanisms supporting effect, the multiple neck formation as well as the lateral contraction hindrance can be distinguished. It is shown that these physical mechanisms lead to changes of the manifestation of PLC bands in the aluminum layer and additionally to multiple localized deformation regions in the intermediate steel layer. Thereby, a 5% improvement in elongation at break for the AL-HC-AL-hybrid in comparison to the monolithic aluminum can be demonstrated. Furthermore, it is shown that the manifestation of the mechanism localization hindrance and thereby the stepped failure behavior can be influenced by the applied structural adhesive.

The experimental results of the HSD-HC-HSD-hybrid demonstrate that the physical mechanisms localization hindrance and bridging effect lead to a change in the strain path of the intermediate HC layer, to stabilization of plastic instabilities of the HC layer and, subsequently, to enlarged uniform elongation. An up to 25% improvement in the uniform elongation and the elongation to break compared to monolithic HC can be achieved by this type of hybridization. An influence of the adhesive properties on the manifestation of the localization hindrance cannot be shown for HSD-HC-HSD-hybrids.

The presented results for HC-HSD-hybrids of the complementary numerical studies demonstrate that theoretically by reinforcing the HC layer (1.0 mm) on one side with an 1.0 mm thick HSD layer or on two sides with 0.6 mm thick HSD layers the uniform elongation and elongation at break of the monolithic HSD can be achieved. Even the single-sided reinforcement with an HSD layer of the thickness of 0.2 mm lead to a uniform elongation improvement of about 20% and a 10% improvement in elongation at break. The studies on both material systems indicate that especially the portions and thereby the thickness ratio of the components is decisive for the onset of plastic instability. This onset of instability is initiating failure of the hybrid. Therefore, as an extension to this manuscript comprehensive investigations on plastic instability in hybrid material systems will be conducted. To identify the main factor influencing the onset of diffuse and local necking, the cross-sections, the forces as well as the strain paths of the individual layers of the hybrid material system will be tracked and evaluated. In the course of these investigations, additionally, the influence of different adhesives as well as the influence of single- or double-sided reinforcement on the start of the localization will be examined in detail.

Implementing a mechanism-based design strategy enables the adjustment of the ductility and also the tensile strength of material combinations. Hence, according to the local requirements, locally tailored properties can be obtained by the hybridization of a base structure with precisely designed patches.

Acknowledgement

The project “Hybride Werkstoffsysteme: Systematische Betrachtung und Bewertung der physikalischen Wirkmechanismen” is supported by a grant from the State Ministry of Science, Research and the Arts of Baden-Württemberg in Germany (Az: 32-7533.-4-113.11/1/1) and BMW Group. The authors are grateful to the financial support through the funding agencies.

References

[1] M.F. Ashby, Materials selection in mechanical design: Das Original mit Uebersetzungshilfen, dt. easy-reading-ausg. d. 3. ed., 1. aufl./hrsg. Alexander Wanner Edition, Easy reading, Elsevier Spektrum Akad. Verl., München, 2007,
[2] D.J. Nestler, Beitrag zum Thema Verbundwerkstoffe - Werkstoffverbunde: Status quo und Forschungsansätze, Universitätsverlag Chemnitz, Chemnitz, 2014.
[3] S. Lee, J. Wadsworth, O.D. Sherby, Tensile properties of laminated composites based on ultrahigh carbon steel, J. Compos. Mater. 25 (1991) 842–853.
[4] O. Bouaziz, J.P. Masse, G. Petitgand, M.X. Huang, A novel strong and ductile TWIP/martensite steel composite, Adv. Eng. Mater. 18 (1) (2016) 56–59. http://dx.doi.org/10.1002/adem.201500113.
[5] C.K. Syn, D.R. Lesuer, J. Wolfenstine, O.D. Sherby, Layer thickness effect on ductile tensile fracture, Metall. Trans. A. 24 (7) (1993) 1647–1653. http://dx.doi.org/10.1007/BF02646603.
[6] T. Koseki, J. Inoue, S. Nambu, Development of multilayer steels for improved combinations of high strength and high ductility, Mater. Trans. 55 (2) (2014) 227–237.
[7] J. Inoue, S. Nambu, Y. Ishimoto, T. Koseki, Fracture elongation of brittle/ductile multilayered steel composites with a strong interface, Scr. Mater. 59 (10) (2008) 1055–1058. http://dx.doi.org/10.1016/j.scriptamat.2008.07.020.
[8] D.R. Lesuer, C.K. Syn, O.D. Sherby, J. Wadsworth, J.J. Lewandowski, W.H. Hunt, Mechanical behaviour of laminated metal composites, Int. Mater. Rev. 41 (5) (1996) 169–197. http://dx.doi.org/10.1179/095066096790151204.
[9] S.L. Semiatin, H.R. Piehler, Deformation of sandwich sheet materials in uniaxial tension, Metall. Trans. A. 10 (1) (1979) 85–96. http://dx.doi.org/10.1007/BF02686411.
[10] P. Lhuissier, J. Inoue, T. Koseki, Strain field in a brittle/ductile multilayered steel composite, Scr. Mater. 64 (10) (2011) 970–973. http://dx.doi.org/10.1016/j.scriptamat.2011.01.048.
[11] S. Nambu, M. Michiuchi, Y. Ishimoto, K. Asakura, J. Inoue, T. Koseki, Transition in deformation behavior of martensitic steel during large deformation under uniaxial tensile loading, Scr. Mater. 60 (4) (2009) 221–224. http://dx.doi.org/10.1016/j.scriptamat.2008.10.007.
[12] M. Ojima, J. Inoue, S. Nambu, P. Xu, K. Akita, H. Suzuki, T. Koseki, Stress partitioning behavior of multilayered steels during tensile deformation measured by in situ neutron diffraction, Scr. Mater. 66 (3–4) (2012) 139–142. http://dx.doi.org/10.1016/j.scriptamat.2011.10.018.
[13] S. Nambu, M. Michiuchi, J. Inoue, T. Koseki, Effect of interfacial bonding strength on tensile ductility of multilayered steel composites, Compos. Sci. Technol. 69 (11–12) (2009) 1936–1941. http://dx.doi.org/10.1016/j.compscitech.2009.04.013.
[14] Dow Automotive AG, Betamate 2090: Technical Datasheet, 2011.
[15] Dow Automotive AG, Betamate 2090 1:1: Technical Datasheet, 2015.
[16] Dow Automotive AG, Betamate 2098: Technical Datasheet, 2011.
[17] DIN — Deutsches Institut für Normung e.V., Prüfung metallischer Werkstoffe - Zugproben, 2009.
[18] M. Maj, W. Oliferuk, Analysis of plastic strain localization on the basis of strain and temperature fields, Arch. Metall. Mater. 57 (4) (2012) 1111–1116. http://dx.doi.org/10.2478/v10172-012-0124-2.
[19] DIN — Deutsches Institut für Normung e.V., Metallische Werkstoffe - Zugversuch - Teil 1: Prüfverfahren bei Raumtemperatur (ISO/DIS 6892-1:2014); Deutsche Fassung prEN ISO 6892-1:2014, 2014.
[20] V. ABAQUS, 6.14 Documentation, 2014.
[21] H. Hooputra, H. Gese, H. Dell, H. Werner, A comprehensive failure model for crashworthiness simulation of aluminium extrusions, Int. J. Crashworthiness 9 (5) (2004) 449–464. http://dx.doi.org/10.1533/ijcr.2004.0289.
[22] H.W. Swift, Plastic instability under plane stress, J. Mech. Phys. Solids 1 (1) (1952) 1–18. http://dx.doi.org/10.1016/0022-5096(52)90002-1.
[23] P. Larour, Strain rate sensitivity of automotive sheet steels: influence of plastic strain, strain rate, temperature, microstructure, bake hardening and pre-strain, Berichte aus dem Institut fur Eisenhuttenkunde, vol. Bd. 2010,1, Shaker, Aachen, 2010, [online-ausg.] Edition.
[24] E.W. Hart, Theory of the tensile test, Acta Mater. 15 (1967) 351–355.
[25] J.J. Jonas, R.A. Holt, C.E. Coleman, Plastic stability in tension and compression, Acta Metall. 24 (10) (1976) 911–918. http://dx.doi.org/10.1016/0001-6160(76)90039-0.
[26] J.W. Hutchinson, K.W. Neale, Influence of strain-rate sensitivity on necking under uniaxial tension, Acta Metall. 25 (1977) 839–846.
[27] J.W. Hutchinson, H. Obrecht, Tensile instabilities in strain-rate dependent materials, Fracture 1 (1977) 101–116.
[28] Forschungsvorhaben P FOSTA 957 / 422 ZN, Experimentelle Kennwertermittlung und Simulation von strukturellen Klebverbindungen mit elastoplastischn und bruchmechanischen Kohäsivelementen: Abschlussbericht, 2015.

[29] A. Kelly, G.J. Davies, The principles of the fibre reinforcement of metals, Metall. Rev. 10 (1) (2013) 1–77. http://dx.doi.org/10.1179/mtlr.1965.10.1.1.
[30] H. Halim, D. Wilkinson, M. Niewczas, The Portevin-Le Chatelier (PLC) effect and shear band formation in an AA5754 alloy, Acta Mater. 55 (12) (2007) 4151–4160. http://dx.doi.org/10.1016/j.actamat.2007.03.007.
[31] P. Penning, Mathematics of the Portevin-Le Chatelier effect, Acta Metall. 20 (10) (1972) 1169–1175. http://dx.doi.org/10.1016/0001-6160(72)90165-4.
[32] Y. Bao, T. Wierzbicki, A comparative study on various ductile crack formation criteria, J. Eng. Mater. Technol. 126 (3) (2004) 314. http://dx.doi.org/10.1115/1.1755244.
[33] Y. Bao, T. Wierzbicki, On fracture locus in the equivalent strain and stress triaxiality space, Int. J. Mech. Sci. 46 (1) (2004) 81–98. http://dx.doi.org/10.1016/j.ijmecsci.2004.02.006.
[34] T. Wierzbicki, Y. Bao, Y.-W. Lee, Y. Bai, Calibration and evaluation of seven fracture models, Int. J. Mech. Sci. 47 (4–5) (2005) 719–743. http://dx.doi.org/10.1016/j.ijmecsci.2005.03.003.
[35] D. Hummelberger, L. Kärger, F. Henning, Evaluation of different hybrid material systems and systematic analysis of their physical mechanisms in terms of fatigue, Mater. Sci. Forum 825-826 (2015) 473–481. http://dx.doi.org/10.4028/www.scientific.net/MSF.825-826.473.
[36] Y. Ohashi, J. Wolfenstine, R. Koch, O.D. Sherby, Fracture behavior of a laminated steel-brass composite in bend tests, Mater. Sci. Eng. A 151 (1992) 37–44.
[37] N.G. Gonzalez-Canche, E.A. Flores-Johnson, J.G. Carrillo, Mechanical characterization of fiber metal laminate based on aramid fiber reinforced polypropylene, Compos. Struct. 172 (2017) 259–266. http://dx.doi.org/10.1016/j.compstruct.2017.02.100.
[38] M. Merzkirch, M. Meissner, V. Schulze, K.A. Weidenmann, Tensile behaviour of spring steel wire reinforced EN AW-6082, J. Compos. Mater. 49 (3) (2015) 261–274. http://dx.doi.org/10.1177/0021998313517581.
[39] M. Merzkirch, M. Meissner, V. Schulze, K.A. Weidenmann, Numerical analysis to study the tensile behaviour of a spring-steel-wire-reinforced aluminium alloy metal matrix composite, J. Compos. Mater. 49 (21) (2015) 2659–2671. http://dx.doi.org/10.1177/0021998314553044.